Suppressive role of SCN4B in the epithelial-mesenchymal transition of lung adenocarcinoma

MENGNAN GUO[1], HE LI[2], ZHIFANG ZHAO[1], YUANYUAN WANG[1], JIAQI TANG[1], BINGHAN ZHONG[1] and YUNXIA ZHAO[1]

[1]Department of Respiratory Medicine, Hebei Medical University Third Hospital, Shijiazhuang, Hebei 050051, P.R. China; [2]Department of Respiratory Medicine, Xiangyang Central Hospital, Affiliated Hospital of Hubei University of Arts and Science, Xiangyang, Hubei 441021, P.R. China

Received September 9, 2025; Accepted January 12, 2026

DOI: 10.3892/or.2026.9073

Abstract. The poor prognosis and high mortality rate of non-small cell lung cancer are largely driven by its aggressive migratory and invasive behavior. Epithelial-mesenchymal transition (EMT) is a central mechanism conferring these malignant traits. The present study examined the expression profile of the sodium channel β4 subunit (*SCN4B*) in lung adenocarcinoma (LUAD) and explored its regulatory role in EMT. Transcriptomic data from The Cancer Genome Atlas were analyzed to compare *SCN4B* expression between LUAD and normal tissues, and to assess its relationship with TNM clinical stage (I-IV), overall survival and diagnostic performance using non-parametric tests, Kaplan-Meier analysis and receiver operating characteristic curves, respectively. Functional enrichment analysis, including Gene Ontology and Kyoto Encyclopedia of Genes and Genomes (KEGG) analysis, and immune cell infiltration profiling were performed on *SCN4B*-associated differentially expressed genes. *In vitro*, the A549 and H1299 LUAD cell lines were engineered to overexpress *SCN4B*. Viability, migration, invasion and apoptosis were evaluated using Cell Counting Kit-8 assays, wound healing assays, Transwell assays and flow cytometry. In addition, western blotting was conducted to assess EMT markers, including E-cadherin, N-cadherin, Vimentin and Snail. The results demonstrated that *SCN4B* expression was markedly reduced in LUAD tissues and low SCN4B expression was associated with unfavorable clinical outcomes. KEGG analysis revealed enrichment of SCN4B-related genes in the 'cell adhesion molecules' pathway, and SCN4B expression levels differed markedly between TNM tumor (T) pathologic stages T1 and T2. Furthermore, SCN4B overexpression suppressed viability, migration and invasion of A549 and H1299 cells, while promoting apoptosis. Western blotting demonstrated upregulation of E-cadherin, and downregulation of N-cadherin, Vimentin and Snail in the *SCN4B* overexpression group compared with the empty vector group, indicating inhibition of EMT. In conclusion, low *SCN4B* expression was associated with poor prognosis in LUAD. Notably, restoring *SCN4B* levels suppressed LUAD cell viability, migration and invasion *in vitro*, accompanied by inhibition of EMT. These findings highlighted *SCN4B* as a potential tumor suppressor and a promising therapeutic target for LUAD.

Correspondence to: Professor Yunxia Zhao, Department of Respiratory Medicine, Hebei Medical University Third Hospital, 139 Ziqiang Road, Shijiazhuang, Hebei 050051, P.R. China
E-mail: 13032609797@163.com

Key words: lung adenocarcinoma, sodium channel β4 subunit, epithelial-mesenchymal transition, invasion, migration, The Cancer Genome Atlas

Introduction

Lung cancer, a malignancy that poses a major threat to human health, is generally classified into two main subtypes: i) Small cell lung cancer; and ii) non-small cell lung cancer (NSCLC) (1), with the latter accounting for ~85% of all cases (2). Although notable progress has been achieved in the treatment of lung cancer, through advances in surgical techniques, refinement of chemoradiotherapy regimens, and the introduction of targeted and immune-based therapies (3), overall survival (OS) remains unsatisfactory, particularly among patients with advanced disease (4). Metastasis is a principal cause of therapeutic failure and mortality in lung cancer (5). Epithelial-mesenchymal transition (EMT) refers to a process in which epithelial cells, under specific physiological or pathological conditions, lose their epithelial characteristics and acquire the phenotype and functional properties of mesenchymal cells (6). During EMT, the expression of epithelial markers, such as E-cadherin, is markedly reduced, whereas mesenchymal markers, including N-cadherin and Vimentin, are upregulated, thereby enhancing cellular migratory and invasive capacities (7,8). Increasing evidence indicates that EMT serves a pivotal role in the initiation, progression, invasion and metastasis of lung cancer. Multiple signaling pathways have been implicated in regulating EMT in lung cancer cells, including the TGF-β pathway (9), Notch pathway (10) and Wnt pathway (11,12). EMT-related transcription factors, such as Snail (13), Twist (14) and zinc-finger E homeobox-binding family members (15), are frequently upregulated in lung

cancer tissues (16). These factors directly repress E-cadherin expression while inducing the expression of mesenchymal markers such as N-cadherin and Vimentin, thereby driving EMT (17). Despite advances in the understanding of the relationship between lung cancer and EMT, numerous mechanistic questions remain to be addressed.

The sodium channel β4 subunit (*SCN4B*) gene encodes a crucial subunit of the voltage-gated sodium channel, serving a key role in cellular electrophysiological functions (18,19). Previous studies have primarily concentrated on its involvement in the nervous system, particularly in relation to neuromuscular disorders (20,21). However, emerging evidence indicates that *SCN4B* may also contribute to pathologies beyond the nervous system, notably in cancer, a major threat to human health. For instance, alterations in *SCN4B* expression have been implicated in modulating tumor cell proliferation and metastasis in colorectal cancer (22). In lung cancer, *SCN4B* expression levels have been reported to be closely associated with tumor aggressiveness and patient prognosis, underscoring its potential influence on disease progression (23). In summary, *SCN4B* was proposed to act as a tumor suppressor by restraining the excessive activation of tumor cell migration.

In the present study, the differential expression of *SCN4B* in lung adenocarcinoma (LUAD) was analyzed and its prognostic significance was evaluated. Based on these findings, Gene Ontology (GO) and Kyoto Encyclopedia of Genes and Genomes (KEGG) pathway enrichment analyses were performed on *SCN4B*-associated differentially expressed genes, alongside immune infiltration profiling. To further elucidate the role of *SCN4B* in suppressing LUAD cell migration and invasion, *SCN4B*-overexpressing cell lines were established. The effect of *SCN4B* on tumor progression was assessed by examining changes in cell viability, migration and invasion. Finally, the effect of *SCN4B* on the EMT process was investigated through the evaluation of EMT-related marker protein expression levels. Based on previous reports (24,25), we hypothesized that SCN4B may be involved in EMT regulation in LUAD, and the working hypothesis is summarized in Fig. 1.

Materials and methods

Data acquisition and preprocessing. Transcriptomic data for The Cancer Genome Atlas (TCGA)-LUAD cohort were obtained from TCGA portal (https://portal.gdc.cancer.gov) using the Spliced Transcripts Alignment to a Reference processing pipeline. Expression profiles were extracted in the transcripts per million format, and paired tumor-adjacent and tumor tissue samples were identified based on matched patient identifiers. In total, 598 samples were included in the analysis, comprising 59 normal lung tissues and 539 LUAD specimens.

Differential expression analysis of SCN4B. Bioinformatics and statistical analyses were performed in R (v4.5.2; R Core Team; http://www.R-project.org/) (26). The expression levels of *SCN4B* in LUAD and adjacent normal tissues were compared using the 'limma' R package (v3.66.0; https://bioconductor.org/packages/release/bioc/html/limma.html). The $\log_2$ fold change ($\log_2$FC) and adjusted P-value (adj. P.Val) were calculated for all genes, and those with $|\log_2 FC|>1$ and adj. P.Val <0.05 were considered significantly differentially expressed. Receiver operating characteristic (ROC) curve analysis was performed using the 'pROC' package (v1.19.0.1; https://cran.r-project.org/package=pROC), and the results were visualized with 'ggplot2' (v4.0.1; https://cran.r-project.org/package=ggplot2) (27).

Visualization of gene expression and correlation analysis. Boxplots were generated using the 'ggplot2' package to display *SCN4B* expression differences between tumor and normal lung tissues. Volcano plots were generated using the 'ggplot2' package to visualize *SCN4B*-associated differentially expressed genes between the *SCN4B* high- and low-expression groups within the TCGA-LUAD tumor cohort. Correlation heatmaps illustrating the relationships between *SCN4B* and selected lung cancer-associated marker genes were created to facilitate visualization of co-expression patterns (28).

GO and KEGG functional enrichment analysis. *SCN4B*-associated differentially expressed genes identified between the *SCN4B* high- and low-expression groups within the TCGA-LUAD tumor cohort ($|\log_2 FC|>1$; adj. P.Val <0.05) were selected for enrichment analysis. GO annotation and KEGG pathway enrichment analysis were performed using the R package 'clusterProfiler' (v4.4.4; https://bioconductor.org/packages/release/bioc/html/clusterProfiler.html) package (29), running under R (v4.5.2; R Core Team; http://www.R-project.org/). Bubble plots generated with the R package 'ggplot2' were used to present the enrichment results.

Prognostic evaluation. OS data for patients with LUAD were obtained from the Gene Expression Profiling Interactive Analysis 2 platform (v2.0; http://gepia2.cancer-pku.cn/#index), while disease-specific survival (DSS) and progression-free interval (PFI) information were sourced from TCGA. Kaplan-Meier survival analysis was conducted, and statistical differences were assessed using the log-rank test. Corresponding P-values were calculated and displayed on the survival plots (30).

Expression validation and prognostic analysis in the Gene Expression Omnibus (GEO; https://www.ncbi.nlm.nih.gov/geo/) dataset

Expression validation. The present study used the GSE31210 (31) (https://www.ncbi.nlm.nih.gov/geo/query/acc.cgi?acc=GSE31210; Affymetrix GPL570; Thermo Fisher Scientific, Inc.) series matrix (robust multi-array average $\log_2$-transformed). *SCN4B* was mapped to probe 236359_at. Samples were grouped as tumor vs. normal (unpaired), and group differences were tested using Welch's t-test; genome-wide analysis employed the linear modeling framework implemented in the limma R/Bioconductor package (version 4.4.4; https://bioconductor.org/packages/release/bioc/html/limma.html) with Benjamini-Hochberg false discovery rate correction.

Prognostic analysis. In GSE31210 (GPL570), OS was used as the endpoint. *SCN4B* expression was extracted using probe 236359_at and patients were dichotomized at the cohort median to generate Kaplan-Meier curves and the number at risk table. Groups were compared using the two-sided log-rank test.

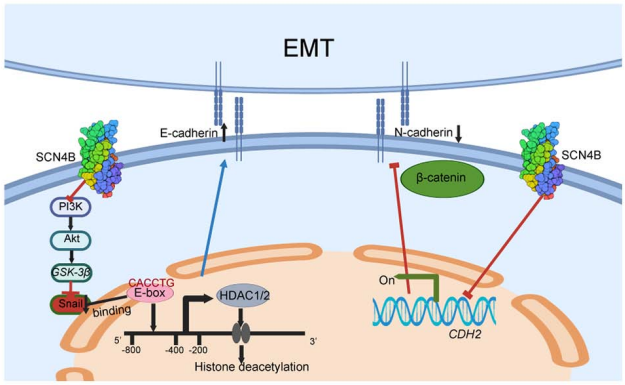

Figure 1. Proposed mechanism of *SCN4B* in the regulation of EMT in lung adenocarcinoma. All activating signaling pathways are indicated by blue solid arrows, while all inhibitory pathways are represented by red T-shaped termination lines. *SCN4B*, sodium channel β4 subunit; EMT, epithelial-mesenchymal transition; CDH2, N-cadherin; HDAC, histone deacetylase.

Clinical association analysis. Clinical information for patients with LUAD, including age, sex, tumor stage and metastatic status, was retrieved from TCGA. The association between *SCN4B* expression and clinical characteristics (such as tumor stage and metastasis) was evaluated using either the χ^2 test or Fisher's exact test (32) (Table I). Bar plots illustrating the relationship between *SCN4B* expression and clinical features were generated with the 'ggplot2' package (33).

Immune infiltration analysis. Correlations between *SCN4B* expression levels and immune cell infiltration scores were assessed, and the results were visualized using lollipop plots generated with the 'ggplot2' package.

Differential expression of SCN4B in tissues. The immunohistochemical expression patterns of SCN4B in adjacent non-tumor and LUAD tissues were obtained from the Human Protein Atlas (HPA) database (https://www.proteinatlas.org/). The analysis was conducted within the 'Tissue' section to explore potential biological implications of *SCN4B* in LUAD.

Cell culture, passaging and cryopreservation. The human LUAD cell lines A549, NCI-H1299, NCI-H1975, PC-9 and HCC827, and the normal human bronchial epithelial cell line BEAS-2B (all from Wuhan Servicebio Technology Co., Ltd.), were maintained in a humidified incubator at 37˚C with 5% CO_2. A549, NCI-H1299 and BEAS-2B cells were cultured in DMEM (Wuhan Servicebio Technology Co., Ltd.), whereas NCI-H1975, PC-9 and HCC827 cells were cultured in RPMI-1640 medium (Wuhan Servicebio Technology Co., Ltd.). All media were supplemented with 10% FBS (Wuhan Servicebio Technology Co., Ltd.) and 1% penicillin-streptomycin (Wuhan Servicebio Technology Co., Ltd.; final concentration 100 U/ml penicillin and 100 µg/ml streptomycin, 100X stock solution). The culture medium was refreshed every 48 h, and cells were passaged at 80-90% confluence (typically every 2-3 days). Cells were cryopreserved at -80˚C overnight and then transferred to liquid nitrogen for long-term storage following standard procedures.

Plasmid transfection and experimental grouping. *SCN4B* overexpression plasmid DNA was transiently transfected into A549 and NCI-H1299 cells using Lipofectamine® 3000 (Invitrogen; Thermo Fisher Scientific, Inc.). The *SCN4B* coding sequence was cloned into the pcDNA3.1(+) backbone at the *Bam*HI/*Eco*RI sites (Sangon Biotech Co., Ltd.). Cells were seeded in 6-well plates (0.3-1x10^5 cells/well) 1 day before transfection. On the day of transfection, 0.5 µg plasmid DNA and 1.5-2.5 µl Lipofectamine 3000 were prepared in serum-free DMEM (Wuhan Servicebio Technology Co., Ltd.) to form transfection complexes according to the manufacturer's instructions, which were then added to the cells. Cells were incubated at 37˚C with 5% CO_2 for 18-24 h (without antibiotics). The transfection efficiency was validated by reverse transcription-quantitative PCR (RT-qPCR) to assess *SCN4B* mRNA expression. Cells were divided into two groups: Vector (empty plasmid) and oe-SCN4B (*SCN4B* overexpression). Subsequent experiments were initiated at 48 h post-transfection, unless otherwise stated.

Cell Counting Kit-8 (CCK-8) viability assay. Cells were seeded into 96-well plates at a density of 5x10^3 cells/well and incubated at 37˚C with 5% CO_2 to allow attachment. At 48 h post-transfection (defined as 0 h for the CCK-8 assay), and at 24, 48 and 72 h thereafter, 10 µl CCK-8 reagent (Wuhan Servicebio Technology Co., Ltd.) was added to each well containing 100 µl culture medium, and plates were incubated for 1-4 h. Absorbance was measured at 450 nm using a microplate reader to quantify the formazan product, which reflects cell viability.

Transwell invasion assays. For the invasion assay, Transwell inserts were precoated with Matrigel (Wuhan Servicebio Technology Co., Ltd.) at 37˚C for 30 min prior to cell seeding. Cells were harvested and resuspended in serum-free DMEM, and a total of 5x10^5 cells in 50 µl were seeded into the upper chamber of each Transwell insert, with the lower chamber filled with DMEM supplemented with 20% FBS (Wuhan Servicebio Technology Co., Ltd.). Each group was prepared in triplicate and cells were incubated at 37˚C with 5% CO_2 for 48 h. Non-invaded cells on the upper surface were gently removed with cotton swabs. The inserts were fixed with 4% paraformaldehyde (Beyotime Biotechnology) for 15 min at room temperature (20-25˚C), stained with crystal violet for 10 min at room temperature and washed three times with PBS. Invaded cells in five random fields (magnification, x100) were imaged using an inverted light microscope and counted using ImageJ software (v1.52a; National Institutes of Health).

Wound healing assay. A549 and H1299 cells were seeded at 5x10^5 cells/well in 6-well plates. Upon reaching ~97% confluence, a scratch was made using a 200-µl pipette tip guided by a ruler to maintain uniform width. Detached cells were removed by PBS washing, followed by incubation in low-serum medium (1% FBS). Images were captured at 0 and 48 h (34) at the same wound site using an inverted light microscope (magnification, x100). The wound closure rate (%) was calculated as: Wound closure rate (%)=[(area at 0 h-area at 48 h)/area at 0 h] x100. The wound area was quantified using ImageJ software (v1.52a;

Table I. Baseline clinical characteristics of patients with lung adenocarcinoma with high and low *SCN4B* expression.

Characteristics	Low *SCN4B* expression, n (%) (n=269)	High *SCN4B* expression, n (%) (n=270)	P-value
Pathologic T stage			0.003
T1	69 (12.9)	107 (20.0)	
T2	166 (31.0)	126 (23.5)	
T3	24 (4.5)	25 (4.7)	
T4	9 (1.7)	10 (1.9)	
Pathologic N stage			0.658
N0	172 (32.9)	178 (34.0)	
N1	54 (10.3)	43 (8.2)	
N2	40 (7.6)	34 (6.5)	
N3	1 (0.2)	1 (0.2)	
Pathologic M stage			0.734
M0	188 (48.2)	177 (45.4)	
M1	12 (3.1)	13 (3.3)	
Pathologic stage			0.164
Stage I	137 (25.8)	159 (29.9)	
Stage II	72 (13.6)	53 (10.0)	
Stage III	45 (8.5)	39 (7.3)	
Stage IV	12 (2.3)	14 (2.6)	
Sex			<0.001
Female	124 (23.0)	165 (30.6)	
Male	145 (26.9)	105 (19.5)	
Age, years			0.005
≤65	144 (27.7)	113 (21.7)	
>65	115 (22.1)	148 (28.5)	
Smoker			0.005
No	27 (5.1)	50 (9.5)	
Yes	235 (44.8)	213 (40.6)	
Anatomic neoplasm subdivision			0.628
Left	100 (19.1)	107 (20.4)	
Right	160 (30.5)	157 (30.0)	

Due to missing or unknown information for certain clinicopathological variables in The Cancer Genome Atlas clinical annotations, the totals for some categories may not sum to the overall cohort size. Percentages were calculated based on the available data for each variable. P-values were calculated using the Pearson χ^2 test or Fisher's exact test, as appropriate. *SCN4B*, sodium channel β4 subunit.

National Institutes of Health). All assays were repeated three times.

RNA extraction and RT-qPCR. Total RNA was extracted from cells using TRIzol® reagent (Beyotime Biotechnology) following the manufacturer's instructions. Briefly, cells at 70-80% confluence (~1x10^6 cells per sample) were lysed in 1 ml TRIzol for RNA extraction. First-strand cDNA was synthesized from 1 μg total RNA using a first-strand cDNA synthesis kit (Beyotime Biotechnology) according to the manufacturer's protocol. qPCR was performed on a Rotor-Gene 3000 real-time PCR system (Gene Company, Ltd.) using SYBR® Green qPCR Master Mix (Beyotime Biotechnology; the fluorophore was SYBR Green I dye provided in the master mix). Each reaction was carried out in a 20 μl volume, and amplification was performed with the following thermocycling conditions: 95˚C for 30 sec, followed by 40 cycles of 95˚C for 5 sec and 60˚C for 30 sec; melt-curve analysis was performed to verify specificity. GAPDH served as the internal control, and relative expression levels were calculated using the $2^{-\Delta\Delta Cq}$ method (35). All qPCR reactions were performed in triplicate (technical replicates). The primer sequences for the target genes were as follows: *SCN4B* forward, 5'-TCTTCCTGCTCCCCG TAAC-3' and reverse, 5'-AATGCGTCACTGCTGTTGTAG-3'; and GAPDH forward, 5'-CTGGGCTACACTGAGCACC-3' and reverse, 5'-AAGTGGTCGTTGAGGGCAATG-3'.

Western blotting. Total cellular proteins were extracted from the collected cell pellets using pre-chilled RIPA lysis buffer (Beijing Solarbio Science & Technology Co., Ltd.)

supplemented with protease and phosphatase inhibitors. Protein concentrations were determined via a BCA assay. A total of 30 μg protein was loaded per lane. Equal amounts of protein samples were separated on 10% SDS-PAGE gels and subsequently transferred onto PVDF membranes. After blocking with 5% non-fat milk at room temperature for 1 h, the membranes were incubated overnight at 4˚C with primary antibodies against *SCN4B* (cat. no. DF4512; 1:1,000), E-cadherin (cat. no. BF0219; 1:1,000), N-cadherin (cat. no. AF5239; 1:1,000), Vimentin (cat. no. BF8006; 1:1,000), Snail (cat. no. AF6032; 1:1,000) and GAPDH (cat. no. AF7021; 1:1,000). Subsequently, the membranes were incubated for 2 h at room temperature with horseradish peroxidase-conjugated secondary antibodies corresponding to the species of the primary antibodies: Anti-rabbit IgG (cat. no. S0001; 1:10,000) or anti-mouse IgG (cat. no. S0002; 1:10,000). All primary and secondary antibodies were purchased from Affinity Biosciences. Protein bands were visualized using a SuperECL Plus chemiluminescent detection kit (LI-COR Biosciences) and imaged with the Bio-Rad ChemiDoc MP system (Bio-Rad Laboratories, Inc.). Band intensities were semi-quantified using ImageJ software (v1.5.2a; National Institutes of Health).

Flow cytometry. Cells were harvested, washed twice with cold PBS and resuspended in 1X Annexin V binding buffer (10 mM HEPES, 140 mM NaCl, 2.5 mM $CaCl_2$, pH 7.4) at ~1x10^6 cells/ml. For each sample, 100 μl of cell suspension was incubated with 5 μl annexin V-FITC and 5 μl PI (Annexin V-FITC Apoptosis Detection Kit; cat. no. C1062; Beyotime Biotechnology) for 15 min at room temperature in the dark. After adding 400 μl binding buffer, samples were analyzed within 1 h on a CytoFLEX flow cytometer (Beckman Coulter, Inc.) using the FITC and PI channels. Data acquisition was performed with CytExpert software (v2.4; Beckman Coulter, Inc.), and data were analyzed with FlowJo (v10.10.0; BD Biosciences). Single-stained and unstained controls were used for compensation. Events were gated to exclude debris and doublets [forward scatter (FSC)/side scatter; FSC-area vs. FSC-height]. No fixation was performed prior to acquisition. Cells were classified as viable (annexin V^-/PI^-), early apoptotic (annexin V^+/PI^-), late apoptotic (annexin V^+/PI^+) or necrotic (annexin V^-/PI^+). The apoptosis rate (%) was calculated as early + late apoptosis.

Statistical analysis. Unless otherwise stated, all experiments were performed in triplicate. Data are presented as the mean ± SD from three independent experiments (n=3), unless otherwise indicated. For non-normally distributed continuous variables, data are presented as the median (interquartile range). Statistical analyses were conducted using GraphPad Prism 8.0 (Dotmatics) and SPSS 26.0 (IBM Corp.). Categorical clinicopathological variables were compared between high and low *SCN4B* expression groups using χ^2 tests or Fisher's exact tests. Survival was analyzed using the Kaplan-Meier method, and differences were evaluated using the log-rank test. For expression analyses based on transcriptomic data, paired data were analyzed using a paired Student's t-test, and unpaired comparisons with unequal variances were analyzed using Welch's t-test. Comparisons among multiple groups were performed using the Kruskal-Wallis test followed by Dunn's multiple comparisons test when data were not normally distributed, whereas two-group comparisons were performed using the Wilcoxon rank-sum test under the same conditions. Spearman's rank correlation was used to assess correlations between SCN4B expression and the expression of selected genes. A two-tailed unpaired Student's t-test was used to analyze the wound healing, Transwell and flow cytometry apoptosis assay data, as well as RT-qPCR (ΔCq values) and western blot densitometric semi-quantification data, comparing between the vector and oe-SCN4B groups. Baseline *SCN4B* expression across multiple lung adenocarcinoma cell lines was compared using one-way ANOVA with Dunnett's post hoc test. The CCK-8 assay data were analyzed using two-way ANOVA with Bonferroni's post hoc test. Correlations between *SCN4B* expression and immune cell infiltration scores were evaluated using Spearman correlation analysis, and the corresponding correlation coefficients and P-values are shown in the figures. ROC curves were generated to assess the diagnostic performance of *SCN4B*. $P<0.05$ was considered to indicate a statistically significant difference.

Results

Differential expression of SCN4B in LUAD. In TCGA-LUAD dataset, 539 tumor samples and 59 adjacent normal tissue samples were analyzed, and 58 matched tumor-normal pairs were available for paired analysis (Fig. 2A). The baseline clinical characteristics of patients with LUAD with high and low *SCN4B* expression are summarized in Table I. Elevated *SCN4B* expression was markedly associated with earlier T stage, sex, age and smoking status, whereas no significant differences were observed in N stage, M stage, overall pathological stage or anatomic neoplasm subdivision.

Expression profiling revealed that *SCN4B* was markedly downregulated in LUAD tissues compared with adjacent normal tissues (Fig. 2A). The external GEO cohort (GSE31210) exhibited significant downregulation of *SCN4B* in tumor vs. normal lung tissues (Fig. 2B). ROC curve analysis (Fig. 2C) indicated that *SCN4B* possessed strong diagnostic potential, with an area under the curve of 0.979 (95% CI, 0.969-0.990).

Differential analysis of SCN4B and related genes. The volcano plot of *SCN4B*-associated differentially expressed genes between the *SCN4B* high- and low-expression groups is shown in Fig. 3A. Spearman's rank correlation analysis was performed to assess the correlation between *SCN4B* and several genes, including *ADAMTS8*, *ADH1B*, *INMT*, *FHL1*, *C1QTNF7*, *MAMDC2*, *ATP1A2*, *TBX4*, *SCN7A*, *TCF21* and *ITGA8* (Fig. 3B). These associations suggest that *SCN4B* and the identified genes may participate in common biological processes (BPs) or signaling pathways, potentially exerting cooperative or reciprocal regulatory effects.

GO and KEGG functional enrichment analysis. GO functional enrichment analysis indicated that the *SCN4B*-associated differentially expressed genes were significantly enriched in BP terms including ‘cell-substrate adhesion’, ‘extracellular structure organization’,

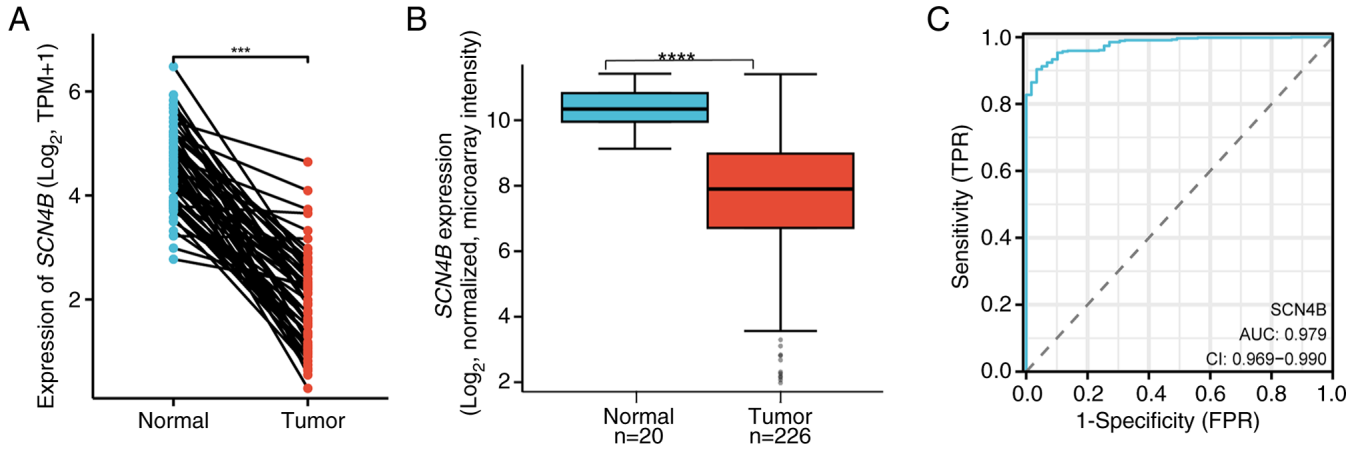

Figure 2. Differential expression analysis of *SCN4B* in LUAD. (A) Differential expression analysis of *SCN4B* in LUAD and adjacent non-tumorous tissue. A paired Student's t-test was used. (B) Gene Expression Omnibus cohort (GSE31210; Affymetrix GPL570): Comparison of *SCN4B* microarray intensity between tumor and normal lung tissues. Welch's t-test was used. (C) Diagnostic receiver operating characteristic curve analysis of *SCN4B*. ***P<0.001, ****P<0.0001. AUC, area under the curve; *SCN4B*, sodium channel β4 subunit; LUAD, lung adenocarcinoma; TPM, transcripts per million; TPR, true positive rate; FPR, false positive rate.

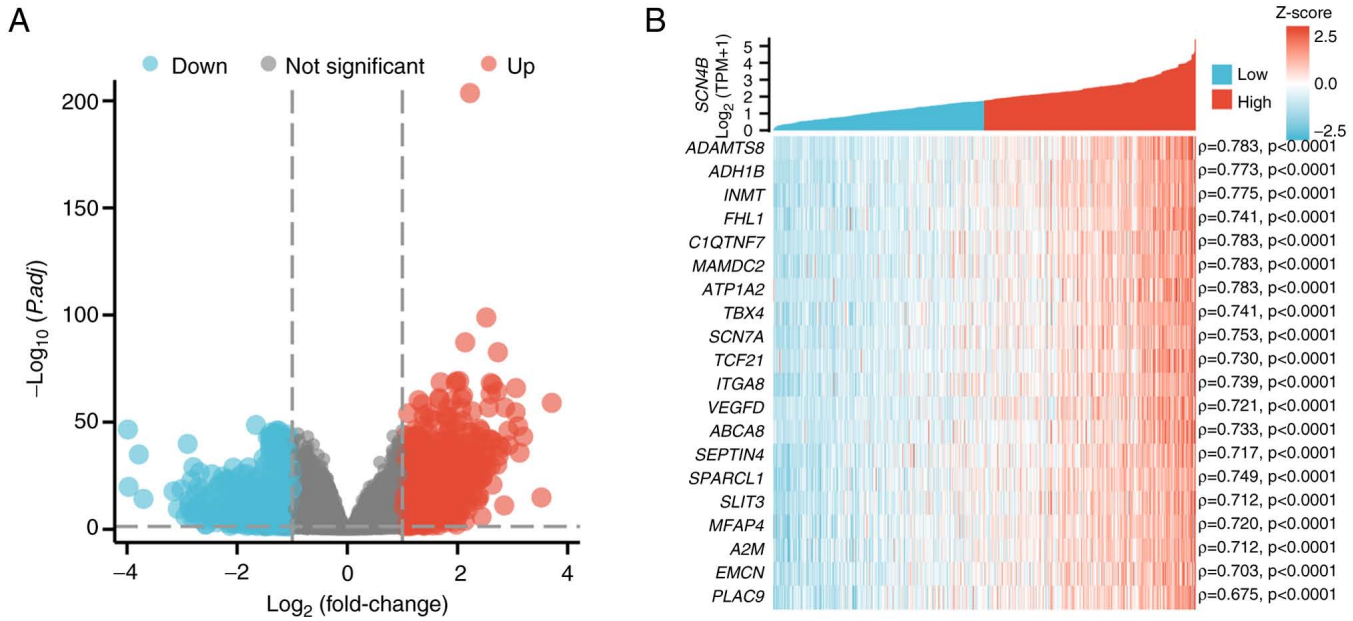

Figure 3. Differentially expressed genes associated with *SCN4B* in lung adenocarcinoma. (A) Volcano plot illustrating SCN4B-associated differentially expressed genes in the dataset. Red dots represent upregulated genes, blue dots indicate downregulated genes and gray dots denote non-significant genes. (B) Spearman's rank correlation analysis between *SCN4B* and selected genes. P.adj, adjusted P-value; *SCN4B*, sodium channel β4 subunit; TPM, transcripts per million.

'extracellular matrix organization' and 'heart morphogenesis'. At the cellular component level, the *SCN4B*-associated differentially expressed genes were mainly associated with 'collagen-containing extracellular matrix', 'cell-cell junction', 'caveola' and 'platelet alpha granule'. In terms of molecular functions (MFs), the *SCN4B*-associated differentially expressed genes were primarily enriched in 'sulfur compound binding', 'glycosaminoglycan binding', 'heparin binding' and 'extracellular matrix structural constituent' (Fig. 4A). In addition, KEGG pathway enrichment analysis showed that the *SCN4B*-associated differentially expressed genes were enriched in pathways such as 'cell adhesion molecules' (CAMs), 'vascular smooth muscle contraction', 'dilated cardiomyopathy', 'hypertrophic cardiomyopathy' and 'arrhythmogenic right ventricular cardiomyopathy' (Fig. 4B).

Immune infiltration analysis of SCN4B. *SCN4B* expression was positively associated with mast cells, eosinophils and immature dendritic cells (iDCs). By contrast, *SCN4B* expression showed a negative correlation with type 2 helper T cells (Th2 cells), natural killer (NK) $CD56^{dim}$ cells, γδ T cells (Tgds) and regulatory T cells (Tregs) (Fig. 5A).

As shown in Fig. 5B, *SCN4B* expression was negatively associated with tumor purity, and weak positive correlations were observed with M2 macrophage and NK cell infiltration

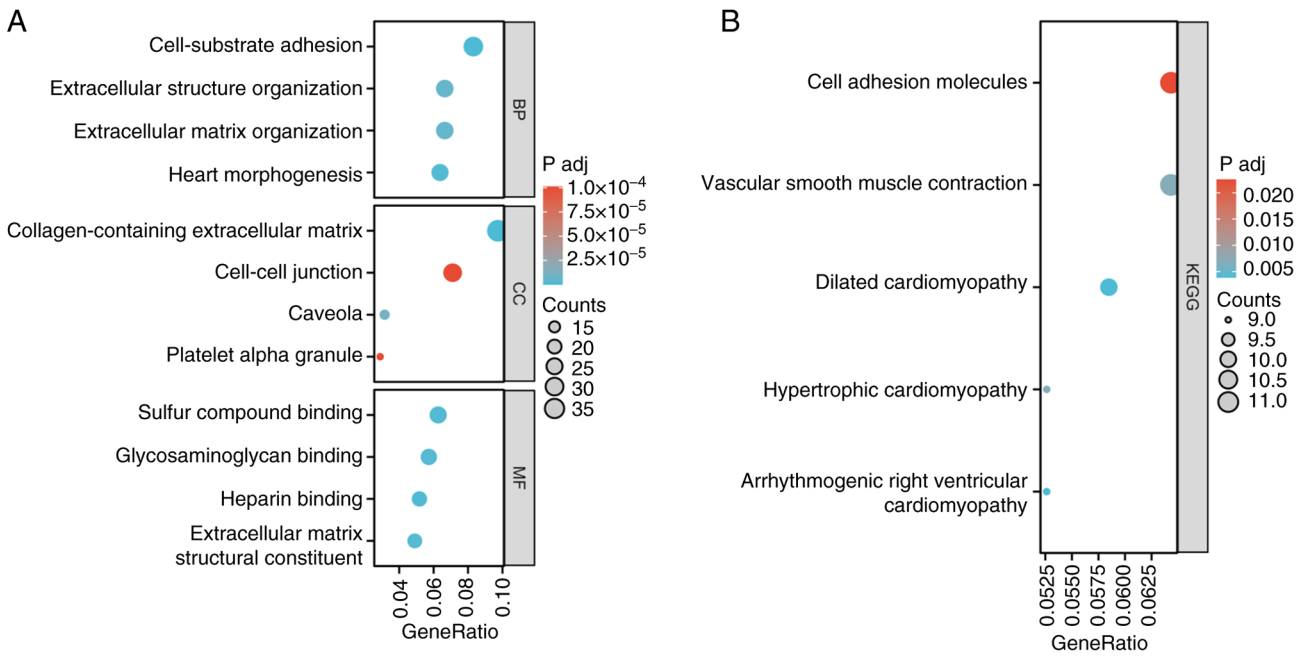

Figure 4. Functional enrichment analysis of SCN4B-associated differentially expressed genes. (A) Gene Ontology functional enrichment analysis based on differences. (B) KEGG functional enrichment analysis. KEGG, Kyoto Encyclopedia of Genes and Genomes; BP, biological process; CC, cellular component; MF, molecular function; P adj, adjusted P-value.

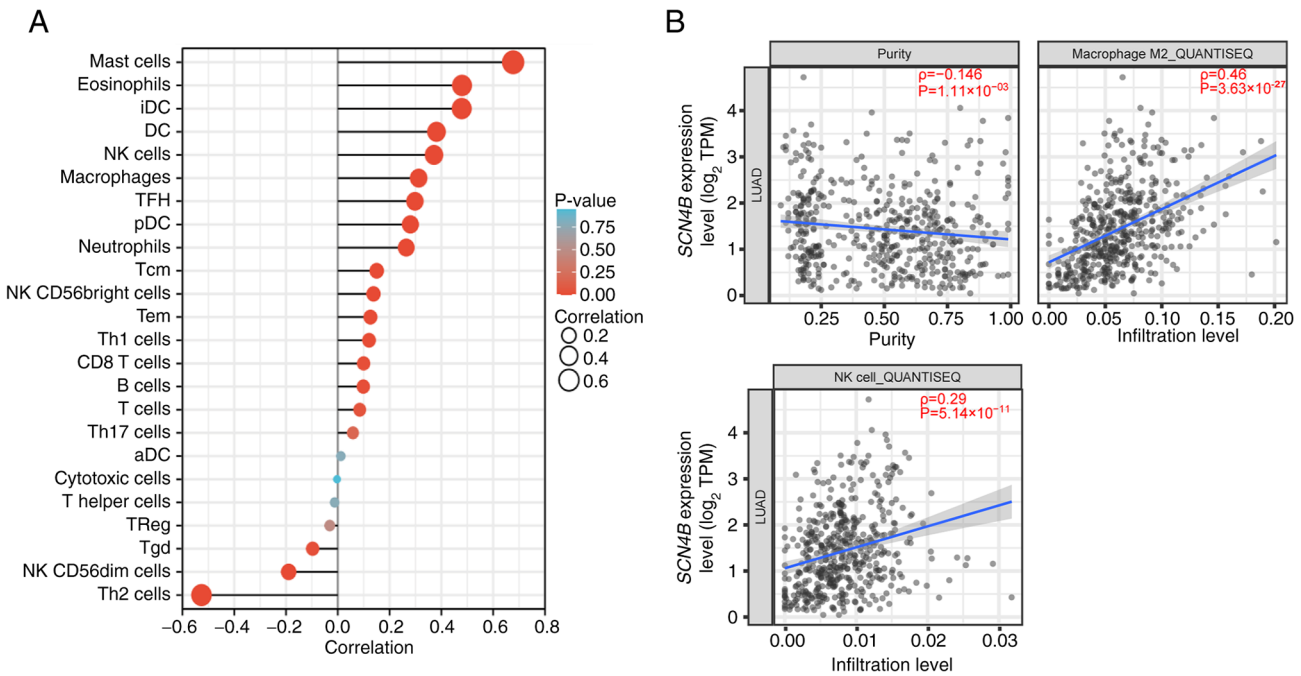

Figure 5. Analysis of immune infiltration related to *SCN4B*. (A) Bubble plot of immune infiltration analysis. (B) Correlation analysis of *SCN4B* expression with tumor purity, M2 macrophage infiltration (quanTIseq) and NK cell infiltration (quanTIseq). Spearman correlation analysis was performed; P-values and P-values are shown. *SCN4B*, sodium channel β4 subunit; NK, natural killer; quanTIseq, quantification of the tumor immune contexture from RNA sequencing; TPM, transcripts per million.

levels estimated by quantification of the tumor immune contexture from RNA sequencing.

SCN4B expression in LUAD and adjacent normal tissues. Analysis using the HPA database revealed that *SCN4B* expression was nearly absent in tumor tissues, whereas detectable expression was observed in adjacent non-tumor tissues (Fig. 6).

Prognostic and clinicopathological association analysis of SCN4B. Patients with high *SCN4B* expression exhibited longer OS and DSS than those with low expression (Fig. 7A and B). High *SCN4B* expression was associated with a longer PFI (Fig. 7C).

In the analysis of *SCN4B* expression across TNM stages, a significant difference was observed between T1 and T2 stages, with markedly reduced expression in T2 tumors. *SCN4B*

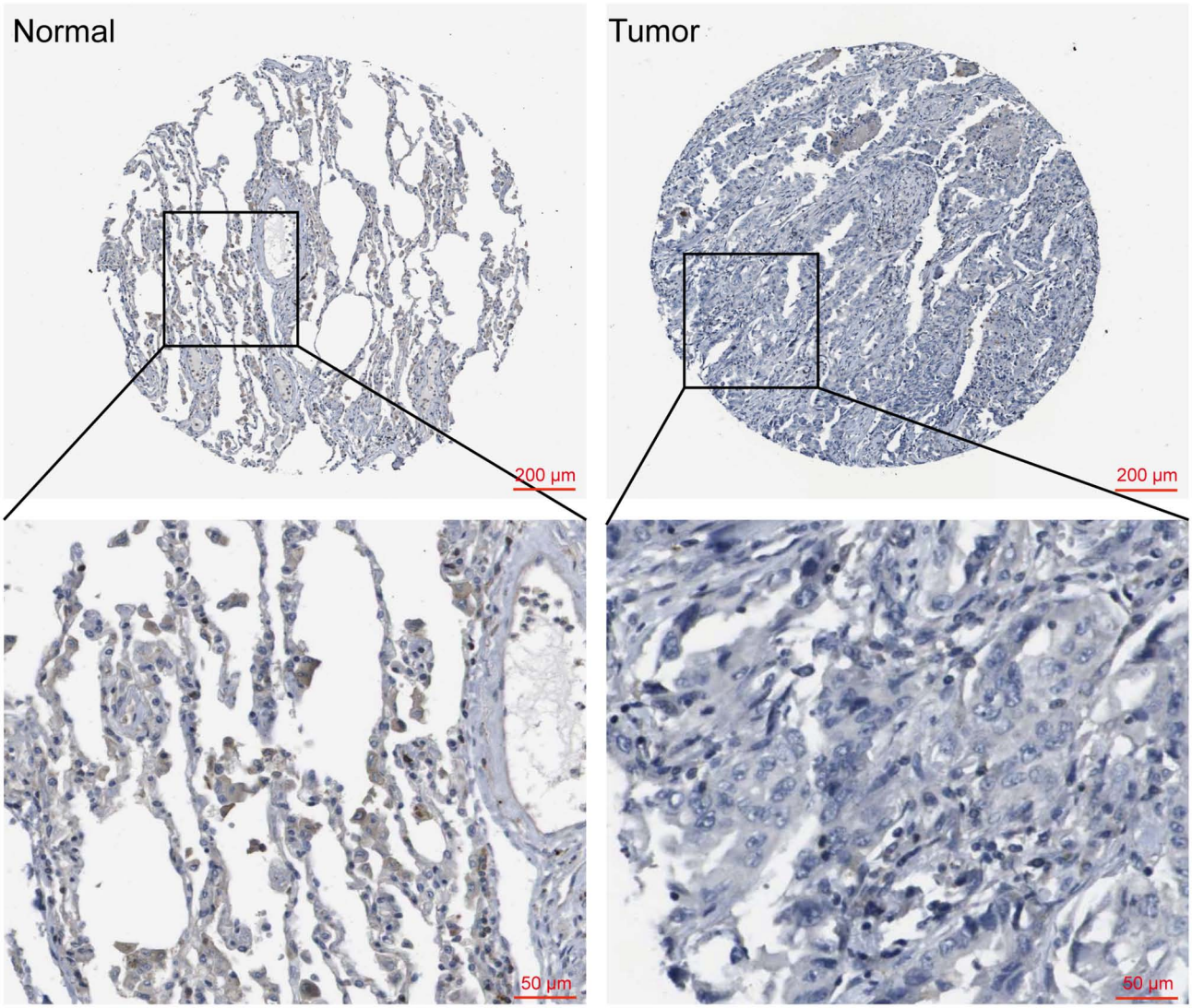

Figure 6. *SCN4B* expression in lung cancer tissues and normal tissues. Immunohistochemical staining images of SCN4B expression in normal lung tissue and lung adenocarcinoma tumor tissue were obtained from the online Human Protein Atlas database (https://www.proteinatlas.org/). The magnification of the first row of images is x100; scale bar, 200 μm; the magnification of the second row of images is x400; scale bar, 50 μm. *SCN4B*, sodium channel β4 subunit.

expression differed between stages T1 and T2. However, no statistically significant differences were observed in stage T3-T4 compared with stages T1 or T2 (Fig. 7D). Furthermore, *SCN4B* expression was not markedly associated with lymph node metastasis, distant metastasis or overall tumor stage (Fig. 7E-G).

External prognostic validation. In the external LUAD cohort GSE31210, high *SCN4B* expression was associated with improved survival. After median dichotomization, Kaplan-Meier curves and the 'number at risk' table displayed below the plot showed a significant difference between groups (Fig. 8).

Baseline SCN4B profiling and model selection. First, SCN4B protein and mRNA levels were screened by western blotting and RT-qPCR in a normal lung-derived cell line and multiple lung cancer cell lines. Using the normal cell line as the reference and normalizing to GAPDH, most cancer cell lines exhibited a marked reduction in *SCN4B* signal. The decrease was most consistent and pronounced in A549 and H1299 cells, which were therefore selected for subsequent functional assays (Fig. 9).

Construction of SCN4B overexpression cell models. *SCN4B* overexpression cell lines were established in A549 and H1299 cells by transfection with an overexpression plasmid. The results showed that the mRNA expression levels of *SCN4B* were markedly increased in the oe-*SCN4B* group compared with the vector group (Fig. 10).

SCN4B reduces lung cancer cell viability and induces apoptosis in LUAD cells. The CCK-8 assay results demonstrated that *SCN4B* overexpression markedly reduced the viability of A549 and H1299 cells in a time-dependent manner, with prolonged exposure leading to stronger inhibitory effects (Fig. 11A).

Flow cytometry analysis using annexin V-FITC/PI double staining revealed that SCN4B overexpression markedly increased the proportion of apoptotic cells (early apoptosis + late apoptosis) in A549 and H1299 LUAD cells (Fig. 11B and C).

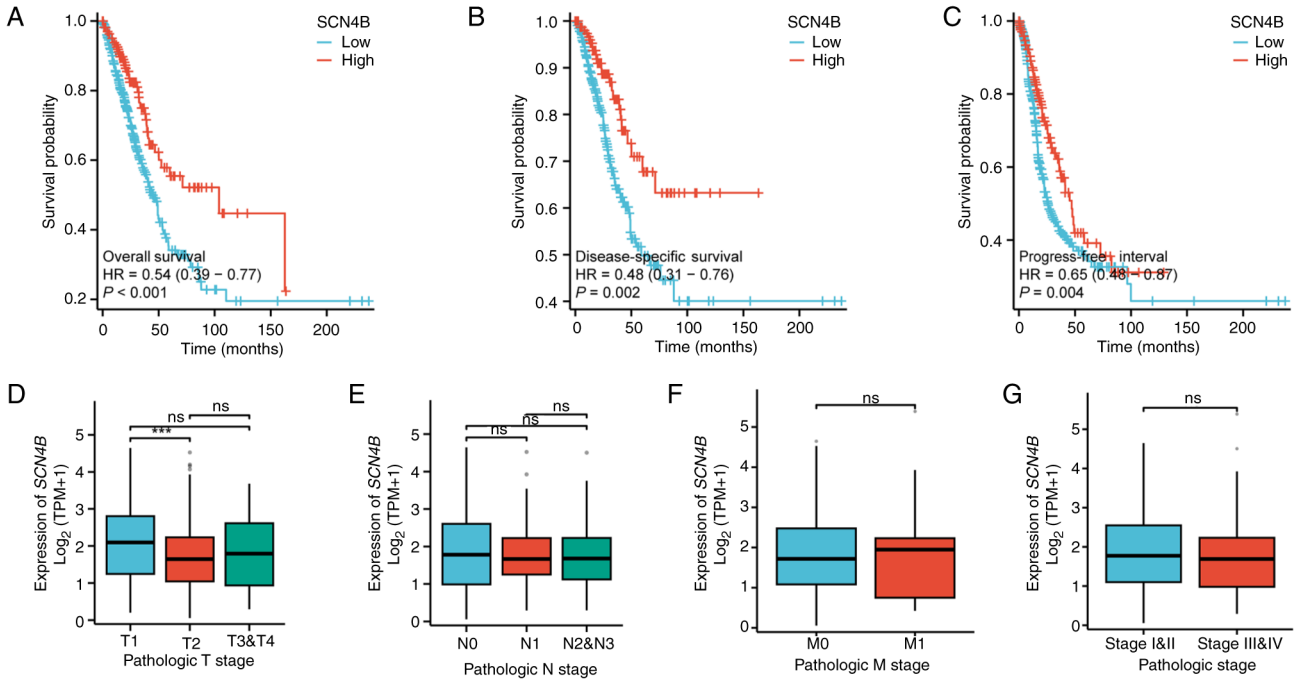

Figure 7. Prognostic analysis and clinical association analysis of *SCN4B*. (A) Kaplan-Meier survival curve for overall survival stratified by *SCN4B* expression. (B) Kaplan-Meier survival curve for disease-specific survival based on *SCN4B* expression levels. (C) Kaplan-Meier survival curve for the progression-free interval in patients with high vs. low *SCN4B* expression. (D) Comparison of *SCN4B* expression across T stages (T1-T4). (E) *SCN4B* expression in patients with or without lymph node metastasis. (F) *SCN4B* expression in patients with or without distant metastasis. (G) *SCN4B* expression across different tumor stages. (D and E) Kruskal-Wallis test. (F and G) Wilcoxon rank-sum test. ***P<0.001. HR, hazard ratio; ns, not significant (P>0.05); *SCN4B*, sodium channel β4 subunit; TPM, transcripts per million.

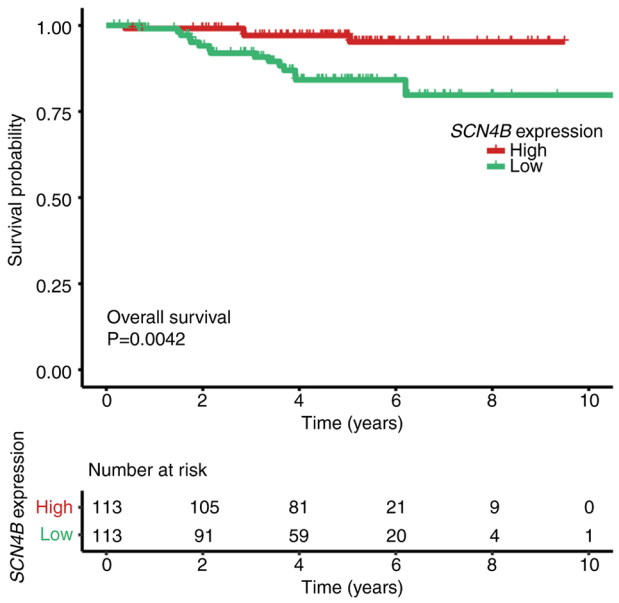

Figure 8. Prognostic association of *SCN4B* in the GSE31210 cohort. Kaplan-Meier curves were generated by stratifying patients into high and low *SCN4B* expression groups using the median expression value as the cutoff. The 'number at risk' table below the plot indicates the counts remaining at risk at each time point. Groups were compared using the two-sided log-rank test (P=0.0042). *SCN4B*, sodium channel β4 subunit.

SCN4B suppresses invasion and migration of LUAD cells. Transwell assay results showed that the number of invasive cells was significantly decreased following *SCN4B* overexpression (Fig. 12A). In addition, wound healing assay results indicated that *SCN4B* overexpression markedly slowed the wound closure rate and markedly reduced the healing area compared with the vector group (Fig. 12B).

Effect of SCN4B on EMT-related marker proteins. Western blot analysis revealed that SCN4B overexpression markedly increased the relative expression levels of E-cadherin, while suppressing the relative expression levels of N-cadherin, Vimentin and Snail (Fig. 13).

Discussion

LUAD is one of the leading causes of tumor-related mortality worldwide, with its high lethality primarily attributed to late-stage diagnosis and highly aggressive biological behavior (36). Among the various mechanisms driving LUAD progression, EMT has been shown to be a central process underlying metastasis and recurrence (37). Therefore, an improved understanding of the molecular regulation of EMT in LUAD is of considerable clinical value.

The present bioinformatics analysis revealed marked downregulation of *SCN4B* expression in LUAD tissues, with low expression markedly associated with unfavorable prognosis. This observation aligns with a previous large-scale analysis reporting a prognostic link between reduced *SCN4B* levels and poor lung cancer outcomes (38).

Kaplan-Meier survival analysis demonstrated that patients with low *SCN4B* expression had a substantially shorter median survival time, while ROC curve analysis indicated

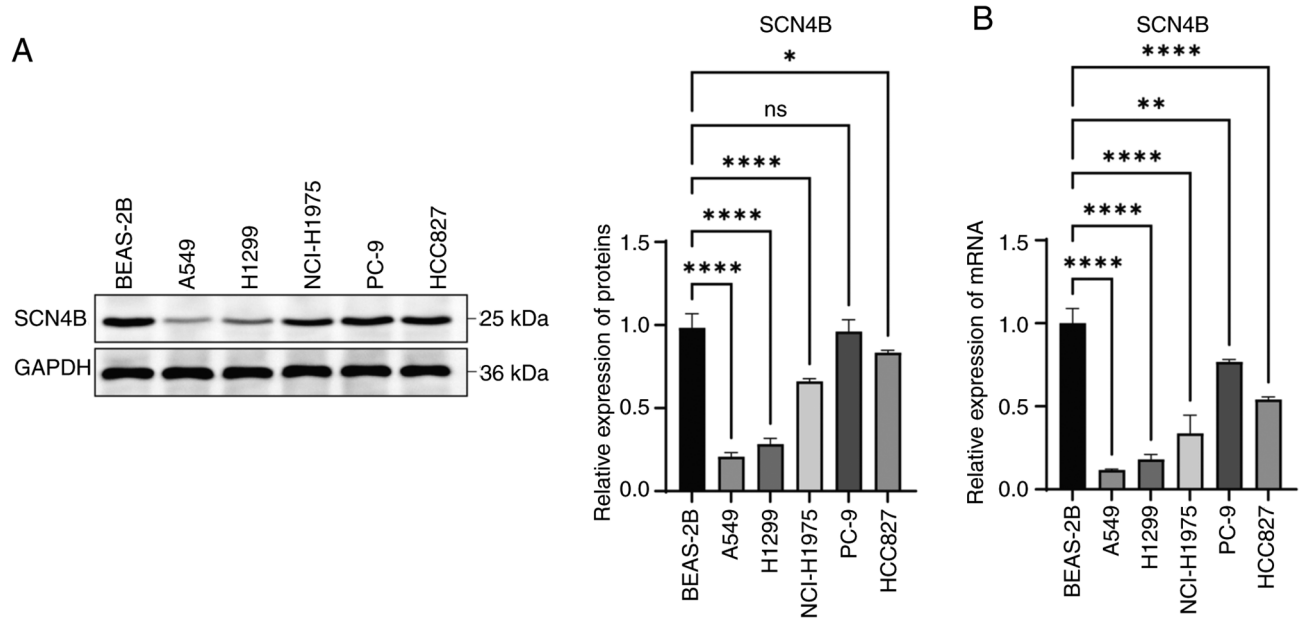

Figure 9. Basal expression of SCN4B across lung cell lines. (A) Representative western blot images: Lane 1, normal lung cells; lanes 2-6, lung cancer cell lines. GAPDH served as the loading control. For densitometric quantification, *SCN4B* was normalized to GAPDH and further normalized to the normal cells (=1). (B) Reverse transcription-quantitative PCR validation in the same panel of distinct cell lines as in (A) (normalized to GAPDH; $2^{-\Delta\Delta Cq}$). One-way ANOVA with Dunnett's post hoc test was used for statistical analysis. N=3 independent experiments. *P<0.05, **P<0.01, ****P<0.0001. ns, not significant (P>0.05); *SCN4B*, sodium channel β4 subunit.

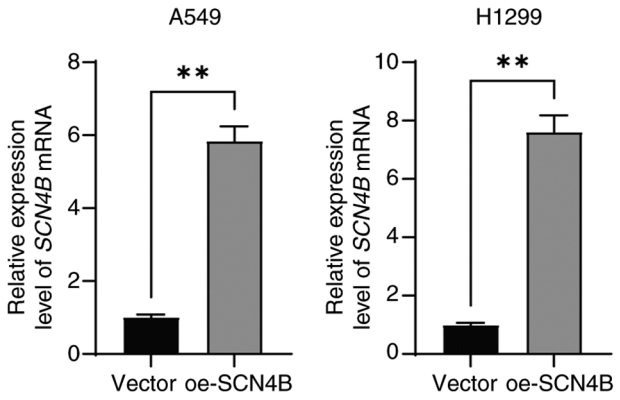

Figure 10. Construction of *SCN4B* overexpression models in A549 and H1299 lung adenocarcinoma cell lines. After transfection with overexpression plasmids for 48 h in A549 and H1299 cells, the relative mRNA expression level changes of *SCN4B* in the cells were detected by reverse transcription-quantitative PCR. Data were analyzed using a two-tailed unpaired Student's t-test. N=3 independent experiments. **P<0.01. *SCN4B*, sodium channel β4 subunit; oe, overexpression.

that *SCN4B* possessed promising diagnostic value in LUAD. Furthermore, analysis by pathological T stage showed that *SCN4B* expression was significantly lower in stage T2 than in stage T1, whereas no statistically significant differences were observed between stage T3-T4 and either stage T1 or stage T2. This trend may indicate that changes in SCN4B expression are closely related to local tumor expansion or primary tumor burden. However, *SCN4B* expression did not significantly differ between groups based on other staging parameters (such as N stage, M stage or pathological stage), which may be due to the limited sample size or may indicate that *SCN4B* primarily participates in early-stage local invasion and proliferation (39). To the best of our knowledge, to date, the biological basis for this stage-specific pattern remains unexplored.

Dysregulated cell proliferation and inhibition of apoptosis are considered key molecular events driving tumor initiation and progression (40,41). Under normal conditions, cell growth is tightly regulated by extracellular cues. However, cancer cells frequently acquire autocrine growth signaling, bypass cell-cycle checkpoints and maintain uncontrolled proliferation (42,43). In the present study, *SCN4B* overexpression in LUAD cell lines (A549 and H1299) markedly reduced the proliferative capacity in a time-dependent manner, as determined by CCK-8 assays. The results showed that *SCN4B* overexpression markedly decreased cell viability in both cell lines, with a time-dependent inhibitory effect. Furthermore, considering that apoptosis evasion is an important mechanism for tumor survival and immune escape (44), annexin V/PI dual-staining flow cytometry was performed to evaluate apoptosis. The results demonstrated that *SCN4B* overexpression markedly induced both early and late apoptosis in LUAD cells. These results suggested that *SCN4B* exerts a tumor-suppressive effect through simultaneous inhibition of proliferation and promotion of apoptosis.

In LUAD, EMT not only drives metastasis but also contributes to chemoresistance and stemness acquisition (45). The Snail family of transcription factors, including Snail1 and Snail2, are key EMT regulators (46). By binding to the E-box elements within the E-cadherin promoter region, they suppress E-cadherin expression, thereby promoting EMT (47). N-cadherin, a mesenchymal cell marker, is upregulated during EMT and is associated with enhanced invasive and migratory abilities (48,49). Vimentin, an intermediate filament protein,

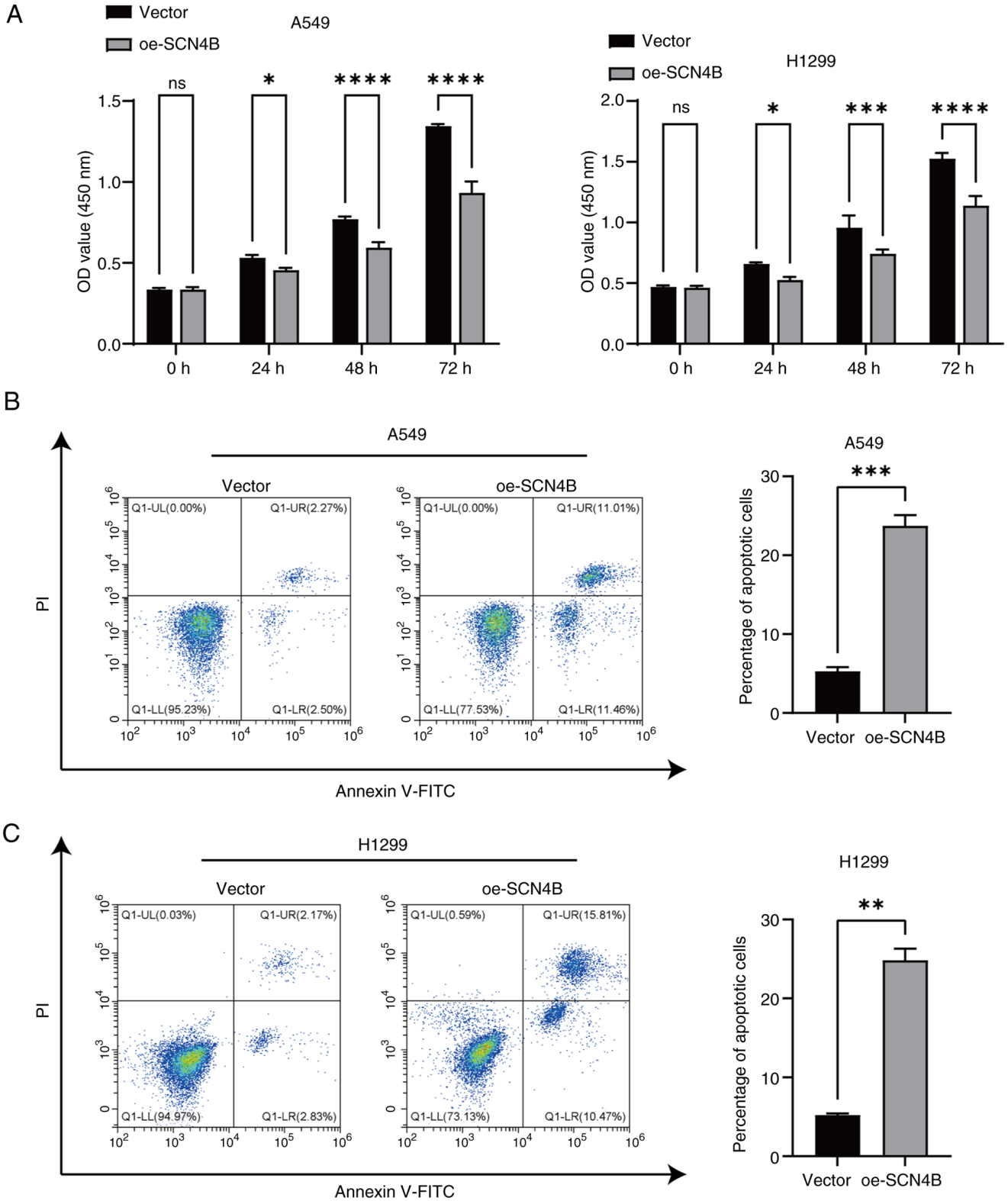

Figure 11. *SCN4B* induces apoptosis and inhibits cell viability. (A) Changes in the viability of A549 and H1299 cells at different time points after transfection (0, 24, 48 and 72 h) were detected using a Cell Counting Kit-8 assay. Data were analyzed using two-way ANOVA with Bonferroni's post hoc test. Changes in the proportion of apoptotic cells after 48 h of transfection in (B) A549 and (C) H1299 cells labeled with PI/annexin V-FITC double staining were detected by flow cytometry. Data were analyzes using a two-tailed unpaired Student's t-test. N=3 independent experiments. *P<0.05, **P<0.01, ***P<0.001, ****P<0.0001. ns, not significant (P>0.05); *SCN4B*, sodium channel β4 subunit; oe, overexpression; OD, optical density.

is another mesenchymal marker whose increased expression during EMT is associated with enhanced motility and invasiveness (50).

The functional assays in the present study demonstrated that *SCN4B* overexpression markedly impaired LUAD cell migration and invasion. Western blot analysis showed that SCN4B

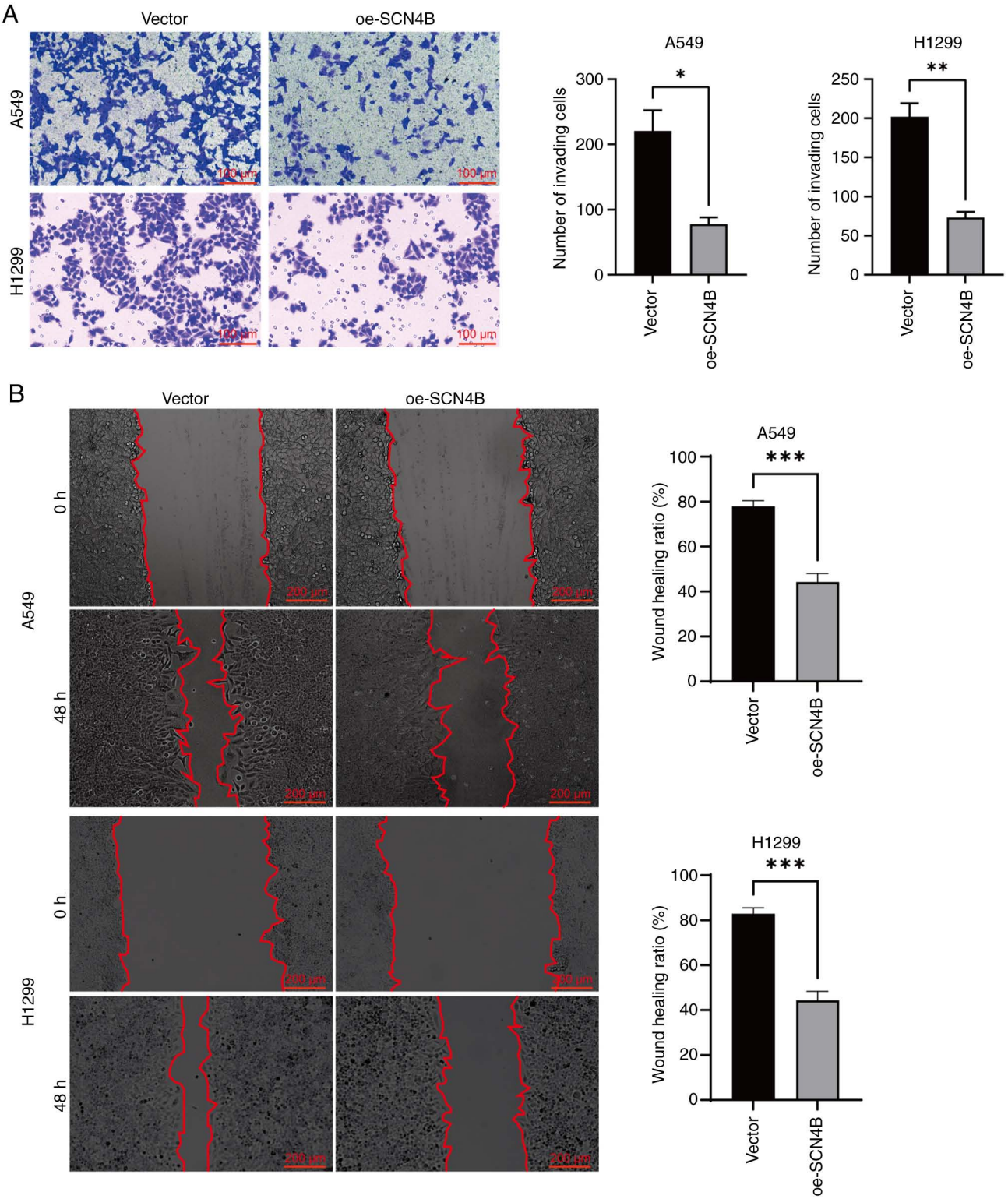

Figure 12. *SCN4B* can inhibit the invasion and migration of lung cancer cells. (A) Changes in the invasion of A549 and H1299 LUAD cells 48 h after transfection with *SCN4B* overexpression plasmid were detected using a Transwell assay (magnification, x100; scale bar, 100 μm). (B) Changes in the migration of A549 and H1299 LUAD cells 48 h after transfection with *SCN4B* overexpression plasmid were detected using a cell scratch assay (magnification, x100; scale bar, 200 μm). Data were analyzed using a two-tailed unpaired Student's t-test. N=3 independent experiments. *P<0.05, **P<0.01, ***P<0.001. *SCN4B*, sodium channel β4 subunit; oe, overexpression; LUAD, lung adenocarcinoma.

elevated E-cadherin expression, while reducing N-cadherin, Vimentin and Snail levels, suggesting a suppressive effect on EMT, potentially via the Snail/E-cadherin axis. Previous work has shown that Snail recruits histone deacetylases to the E-cadherin promoter, modulating H3/H4 acetylation and silencing transcription, providing a plausible mechanism for *SCN4B*-mediated EMT inhibition (41). Taken together, the present results and previous reports (24,25) supported the proposed schematic model whereby SCN4B may regulate EMT in LUAD (Fig. 1).

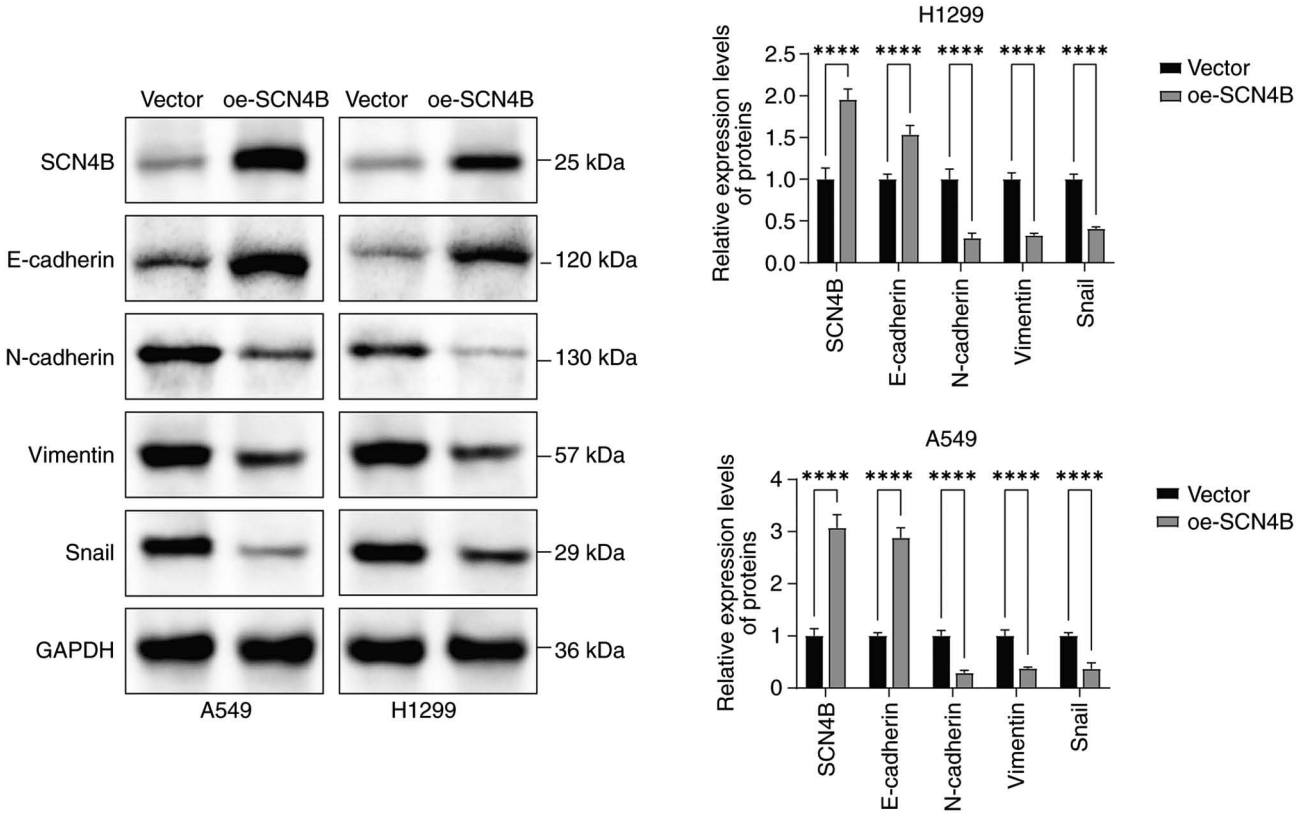

Figure 13. *SCN4B* can inhibit the epithelial-mesenchymal transition process of LUAD cells. The relative protein expression levels of SCN4B, E-cadherin, N-cadherin, Vimentin and Snail in A549 and H1299 LUAD cells 48 h after transfection with SCN4B overexpression plasmid were detected by western blotting. Data were analyzed using a two-tailed unpaired Student's t-test for each protein. N=3 independent experiments. ****P<0.0001. SCN4B, sodium channel β4 subunit; oe, overexpression; LUAD, lung adenocarcinoma.

In the LUAD cell models used in the present study, *SCN4B* overexpression attenuated EMT and invasive behavior, suggesting that its downstream effects may involve several key signaling pathways. Among the classical EMT-inducing cascades, the TGF-β/Smad axis is a major driver of epithelial plasticity, invasive growth and treatment resistance in NSCLC. TGF-β receptor signaling promotes the disassembly of tight junctions, reorganization of the actin cytoskeleton and induction of EMT-related transcription factors such as Snail (51). Previous studies have indicated that *SCN4B* participates in the regulation of cell adhesion and cytoskeletal dynamics (52,53). In the present study, *SCN4B* overexpression increased E-cadherin expression, while reducing N-cadherin, Vimentin and Snail expression. These findings support the hypothesis that *SCN4B* may dampen TGF-β-induced EMT in LUAD cells. Biologically, such an effect would be expected to reduce EMT plasticity and local invasiveness of tumor cells and to alleviate the development of an immunosuppressive, therapy-resistant tumor microenvironment driven by chronic TGF-β signaling, thereby collectively constraining tumor progression.

The Wnt/β-catenin pathway represents another critical signaling cascade that promotes EMT, maintenance of stem-like properties and metastatic spread in lung cancer. Under physiological conditions, β-catenin is sequestered at adherens junctions through binding to E-cadherin. When E-cadherin is lost, β-catenin accumulates in the nucleus and activates Wnt target genes (54). In TCGA-LUAD, enrichment analysis of SCN4B-associated differentially expressed genes highlighted adhesion-related processes, including the KEGG 'cell adhesion molecules' pathway, and in the *in vitro* experiments, SCN4B overexpression increased E-cadherin expression, suggesting that *SCN4B* may indirectly limit sustained activation of canonical Wnt/β-catenin signaling by stabilizing the membrane E-cadherin/β-catenin complex. Integrating these observations, a unified and testable working model in which *SCN4B* functions as a membrane-associated 'brake' was proposed. On the one hand, it attenuates TGF-β/Smad signaling by restricting TGF-β1-induced Smad2/3 phosphorylation and the upregulation of EMT transcription factors (52). On the other hand, it suppresses canonical Wnt/β-catenin signaling by stabilizing epithelial cell-cell junctions, reducing nuclear β-catenin accumulation and lowering T-cell factor/lymphoid enhancer factor reporter activity (55). This integrated model can be evaluated by combining TGF-β1 stimulation and pharmacologic modulation of the Wnt pathway in *SCN4B*-manipulated LUAD cells, together with TCF/LEF-dependent luciferase reporter assays using the TOPflash reporter (containing wild-type TCF/LEF-binding sites) and the FOPflash (containing mutated TCF/LEF-binding sites) mutant control, and analyses of Smad2/3, EMT markers and β-catenin expression and subcellular localization (56). Given that both TGF-β and Wnt/β-catenin pathways are tightly linked to EMT plasticity, stem-like tumor cell subpopulations, metastatic colonization and resistance to systemic therapy, the regulation of these pathways by *SCN4B* may have important implications

for the biological aggressiveness and clinical behavior of LUAD (56,57).

GO and KEGG enrichment analyses of *SCN4B*-associated differentially expressed genes between *SCN4B*-high and *SCN4B*-low LUAD samples were performed to investigate the potential role of *SCN4B* in post-transcriptional regulation and in modulating cellular structure and function during the EMT process. In TCGA-LUAD dataset, GO enrichment analysis revealed that *SCN4B*-associated differentially expressed genes were markedly enriched in BP terms including 'cell-substrate adhesion', 'extracellular structure organization' and 'extracellular matrix organization'. KEGG pathway analysis further demonstrated that these genes were markedly enriched in the 'cell adhesion molecules' pathway. The dynamic balance between microtubule polymerization and depolymerization is a crucial mechanism for maintaining cytoskeletal stability and regulating the migratory capacity of cancer cells (58). The enrichment of *SCN4B*-associated differentially expressed genes in the 'cell adhesion molecules' pathway, involving key adhesion molecules such as E-cadherin and integrins, suggests that *SCN4B* may interfere with the EMT process by modulating intercellular junction structures (such as adherens junctions and desmosomes), thereby inhibiting the invasion and metastasis of LUAD cells (59,60).

In addition, marked enrichment of 'glycosaminoglycan binding' in the MF category was observed in the present study. Glycosaminoglycans, covalently linked to proteins to form proteoglycans, are ubiquitous across mammalian cells, and are present on membranes, in the intracellular space and within the extracellular matrix (ECM). By interacting with a wide range of ligands, they participate in multiple physiological and pathological events, including cancer (61). In the present study, the MF term 'glycosaminoglycan binding' was markedly enriched, suggesting that *SCN4B* may influence the remodeling of the tumor microenvironment and regulate pro-tumorigenic signaling pathways by modulating ECM components.

Immune profiling revealed a positive association between *SCN4B* expression and mast cells, eosinophils and iDCs, but an inverse correlation with Th2 cells, NK $CD56^{dim}$ cells and Tgds. Such patterns suggest that *SCN4B* may act as an immune microenvironment regulator by shaping immune cell infiltration profiles. Given that the tumor microenvironment is integral to cancer initiation, progression, metastasis and therapeutic response, the infiltration landscape of immune cells has direct implications for prognosis (62,63).

Despite the promising findings, the present study has several limitations that must be acknowledged. First, most conclusions were drawn from association analyses based on publicly available transcriptomic datasets, which may introduce selection bias and cannot fully reflect protein-level regulation. Second, the *in vitro* validation was limited to a small number of LUAD cell lines, and thus, may not capture the heterogeneity of the disease. Third, *in vivo* evidence from animal models is still lacking, which restricts the translational interpretation of *SCN4B* function in lung tumor progression. Future research should therefore include validation in larger independent clinical cohorts, incorporate proteomic and *in vivo* functional assays, and explore the underlying molecular mechanisms by which *SCN4B* regulates EMT and tumor metastasis. Addressing these aspects will provide a more comprehensive understanding of *SCN4B* and strengthen its potential as a prognostic biomarker and therapeutic target in LUAD.

In conclusion, low *SCN4B* expression was closely associated with poor prognosis, whereas its high expression may suppress LUAD cell proliferation, migration and invasion by negatively regulating the EMT process.

Acknowledgements

Not applicable.

Funding

No funding was received.

Availability of data and materials

The data generated in the present study are included in the figures and/or tables of this article.

Authors' contributions

MG performed the experiments, collected the data and drafted the manuscript. HL contributed to preliminary research and data analysis. ZZ and YW contributed to the conception and methodology of the study, provided technical input for experimental design and troubleshooting, and critically revised the manuscript for important intellectual content. JT and BZ participated in experimental implementation. YZ conceived and designed the study, and was responsible for overall supervision. MG and HL confirm the authenticity of all the raw data. All authors read and approved the final manuscript.

Ethics approval and consent to participate

Not applicable.

Patient consent for publication

Not applicable.

Competing interests

The authors declare that they have no competing interests.

References

1. Zheng M: Classification and pathology of lung cancer. Surg Oncol Clin N Am 25: 447-468, 2016.
2. Mithoowani H and Febbraro M: Non-small-cell lung cancer in 2022: A review for general practitioners in oncology. Curr Oncol 29: 1828-1839, 2022.
3. Hirsch FR, Scagliotti GV, Mulshine JL, Kwon R, Curran WJ, Wu YL and Paz-Ares L: Lung cancer: Current therapies and new targeted treatments. Lancet 389: 299-311, 2017.
4. Jonna S and Subramaniam DS: Molecular diagnostics and targeted therapies in non-small cell lung cancer (NSCLC): An update. Discov Med 27: 167-170, 2019.
5. Zhang Y, Chen M, Fang X, Han Y and Li Y: Progression and metastasis of lung cancer: Clinical features, molecular mechanisms, and clinical managements. Medcomm 6: e70477, 2025.
6. Manfioletti G and Fedele M: Epithelial-mesenchymal transition (EMT). Int J Mol Sci 24: 11386, 2023.

7. Manfioletti G and Fedele M: Epithelial-mesenchymal transition (EMT) 2021. Int J Mol Sci 23: 5848, 2022.
8. Jiang Y, Han Q, Zhao H and Zhang J: Promotion of epithelial-mesenchymal transformation by hepatocellular carcinoma-educated macrophages through Wnt2b/β-catenin/c-Myc signaling and reprogramming glycolysis. J Exp Clin Canc Res 40: 13, 2021.
9. Lin YT and Wu KJ: Epigenetic regulation of epithelial-mesenchymal transition: Focusing on hypoxia and TGF-β signaling. J Biomed Sci 27: 39, 2020.
10. Shi Q, Xue C, Zeng Y, Yuan X, Chu Q, Jiang S, Wang J, Zhang Y, Zhu D and Li L: Notch signaling pathway in cancer: From mechanistic insights to targeted therapies. Signal Transduct Tar 9: 128, 2024.
11. Ang HL, Mohan CD, Shanmugam MK, Leong HC, Makvandi P, Rangappa KS, Bishayee A, Kumar AP and Sethi G: Mechanism of Epithelial-mesenchymal transition in cancer and its regulation by natural compounds. Med Res Rev 43: 1141-1200, 2023.
12. Xue W, Yang L, Chen C, Ashrafizadeh M, Tian Y and Sun R: Wnt/β-catenin-driven EMT regulation in human cancers. Cell Mol Life Sci 81: 79, 2024.
13. Wei P, Zhang N, Wang Y, Li D, Wang L, Sun X, Shen C, Yang Y, Zhou X and Du X: FOXM1 promotes lung adenocarcinoma invasion and metastasis by upregulating SNAIL. Int J Biol Sci 11: 186-198, 2015.
14. Pan J, Fang S, Tian H, Zhou C, Zhao X, Tian H, He J, Shen W, Meng X, Jin X and Gong Z: lncRNA JPX/miR-33a-5p/Twist1 axis regulates tumorigenesis and metastasis of lung cancer by activating Wnt/β-catenin signaling. Mol Cancer 19: 9, 2020.
15. Clarhaut J, Gemmill RM, Potiron VA, Ait-Si-Ali S, Imbert J, Drabkin HA and Roche J: ZEB-1, a repressor of the semaphorin 3F tumor suppressor gene in lung cancer cells. Neoplasia 11: 157-166, 2009.
16. Wang X, Li M, Yin J, Fang J, Ying Y, Ye T, Zhang F, Ma S, Qin H and Liu X: Emetine dihydrochloride alleviated radiation-induced lung injury through inhibiting EMT. J Cell Mol Med 27: 3839-3850, 2023.
17. Chanvorachote P, Petsri K and Thongsom S: Epithelial to mesenchymal transition in lung cancer: Potential EMT-Targeting natural product-derived compounds. Anticancer Res 42: 4237-4246, 2022.
18. Al-Ward H, Liu CY, Liu N, Shaher F, Al-Nusaif M, Mao J and Xu H: Voltage-gated sodium channel β1 Gene: An overview. Hum Hered 85: 101-109, 2020.
19. Lewis AH and Raman IM: Resurgent current of voltage-gated Na(+) channels. J Physiol 592: 4825-4838, 2014.
20. Ślęczkowska M, Almomani R, Marchi M, Salvi E, de Greef B, Sopacua M, Hoeijmakers J, Lindsey P, Waxman SG, Lauria G, *et al*: Peripheral ion channel genes screening in painful small fiber neuropathy. Int J Mol Sci 23: 14095, 2022.
21. Lu Y, Yu W, Xi Z, Xiao Z, Kou X and Wang XF: Mutational analysis of SCN2B, SCN3B and SCN4B in a large Chinese Han family with generalized tonic-clonic seizure. Neurol Sci 31: 675-677, 2010.
22. Dai W, Zhou J, Wang H, Zhang M, Yang X and Song W: miR-424-5p promotes the proliferation and metastasis of colorectal cancer by directly targeting SCN4B. Pathol Res Pract 216: 152731, 2020.
23. Li X, Chen W, Jiang S, Zhang L, Huang H, Ji Y, Ni Q and Ling C: Low expression of SCN4B predicts poor prognosis in Non-small cell lung cancer. Curr Cancer Drug Targets 25: 445-466, 2025.
24. Peinado H, Ballestar E, Esteller M and Cano A: Snail mediates E-cadherin repression by the recruitment of the Sin3A/histone deacetylase 1 (HDAC1)/HDAC2 complex. Mol Cell Biol 24: 306-319, 2004.
25. Ma Q, Ye S, Liu H, Zhao Y, Mao Y and Zhang W: HMGA2 promotes cancer metastasis by regulating epithelial-mesenchymal transition. Front Oncol 14: 1320887, 2024.
26. R Core Team R: A language and environment for statistical computing. R Foundation for Statistical Computing, Vienna, Austria, 2025. URL http://www.R-project.org/.
27. Hughes G, Kopetzky J and McRoberts N: Mutual information as a performance measure for binary predictors characterized by both ROC curve and PROC curve analysis. Entropy (Basel) 22: 938, 2020.
28. Gustavsson EK, Zhang D, Reynolds RH, Garcia-Ruiz S and Ryten M: Ggtranscript: An R package for the visualization and interpretation of transcript isoforms using ggplot2. Bioinformatics 38: 3844-3846, 2022.
29. Wu X, Sui Z, Zhang H, Wang Y and Yu Z: Integrated analysis of lncRNA-mediated ceRNA network in lung adenocarcinoma. Front Oncol 10: 554759, 2020.
30. Hess AS and Hess JR: Kaplan-Meier survival curves. Transfusion 60: 670-672, 2020.
31. Yamauchi M, Yamaguchi R, Nakata A, Kohno T, Nagasaki M, Shimamura T, Imoto S, Saito A, Ueno K, Hatanaka Y, *et al*: Epidermal growth factor receptor tyrosine kinase defines critical prognostic genes of stage I lung adenocarcinoma. PLoS One 7: e43923, 2012.
32. Feng X, Zahed H, Onwuka J, Callister M, Johansson M, Etzioni R and Robbins HA: Cancer stage compared with mortality as end points in randomized clinical trials of cancer screening: A systematic review and Meta-analysis. JAMA 331: 1910-1917, 2024.
33. Qin H, Lu H, Qin C, Huang X, Peng K, Li Y, Lan C, Bi A, Huang Z, Wei Y, *et al*: Pan-cancer analysis suggests that LY6H is a potential biomarker of diagnosis, immunoinfiltration, and prognosis. J Cancer 15: 5515-5539, 2024.
34. Wang Y, Wang H, Pan T, Li L, Li J and Yang H: STIM1 silencing inhibits the migration and invasion of A549 cells. Mol Med Rep 16: 3283-3289, 2017.
35. Livak KJ and Schmittgen TD: Analysis of relative gene expression data using real-time quantitative PCR and the 2(-Delta Delta C(T)) method. Methods 25: 402-408, 2001.
36. Albuquerque C, Manguinhas R, Costa JG, Gil N, Codony-Servat J, Castro M, Miranda JP, Fernandes AS, Rosell R and Oliveira NG: A narrative review of the migration and invasion features of non-small cell lung cancer cells upon xenobiotic exposure: Insights from in vitro studies. Transl Lung Cancer Res 10: 2698-2714, 2021.
37. Guo Q, Yu W, Tan J, Zhang J, Chen J, Rao S, Guo X and Cai K: Remodelin delays non-small cell lung cancer progression by inhibiting NAT10 via the EMT pathway. Cancer Med 13: e7283, 2024.
38. Liu X, Chen Y, Li Y, Petersen RB and Huang K: Targeting mitosis exit: A brake for cancer cell proliferation. Biochim Biophys Acta Rev Cancer 1871: 179-191, 2019.
39. Venugopal N, Yeh J, Kodeboyina SK, Lee TJ, Sharma S, Patel N and Sharma A: Differences in the early stage gene expression profiles of lung adenocarcinoma and lung squamous cell carcinoma. Oncol Lett 18: 6572-6582, 2019.
40. Seetharaman S and Etienne-Manneville S: Cytoskeletal crosstalk in cell migration. Trends Cell Biol 30: 720-735, 2020.
41. Biswas KH: Molecular Mobility-mediated regulation of E-cadherin adhesion. Trends Biochem Sci 45: 163-173, 2020.
42. Morana O, Wood W and Gregory CD: The apoptosis paradox in cancer. Int J Mol Sci 23: 1328, 2022.
43. Moyer A, Tanaka K and Cheng EH: Apoptosis in cancer biology and therapy. Annu Rev Pathol 20: 303-328, 2025.
44. Yang S, Zhang D, Sun Q, Nie H, Zhang Y, Wang X, Huang Y and Sun Y: Single-cell and spatial transcriptome profiling identifies the transcription factor BHLHE40 as a driver of EMT in metastatic colorectal cancer. Cancer Res 84: 2202-2217, 2024.
45. Corso G, Figueiredo J, De Angelis SP, Corso F, Girardi A, Pereira J, Seruca R, Bonanni B, Carneiro P, Pravettoni G, *et al*: E-cadherin deregulation in breast cancer. J Cell Mol Med 24: 5930-5936, 2020.
46. Na TY, Schecterson L, Mendonsa AM and Gumbiner BM: The functional activity of E-cadherin controls tumor cell metastasis at multiple steps. Proc Natl Acad Sci USA 117: 5931-5937, 2020.
47. Osuka S, Zhu D, Zhang Z, Li C, Stackhouse CT, Sampetrean O, Olson JJ, Gillespie GY, Saya H, Willey CD and Van Meir EG: N-cadherin upregulation mediates adaptive radioresistance in glioblastoma. J Clin Invest 131: e136098, 2021.
48. Gerber TS, Ridder DA, Goeppert B, Brobeil A, Stenzel P, Zimmer S, Jakel J, Metzig MO, Schwab R, Martin SZ, *et al*: N-cadherin: A diagnostic marker to help discriminate primary liver carcinomas from extrahepatic carcinomas. Int J Cancer 154: 1857-1868, 2024.
49. Ridge KM, Eriksson JE, Pekny M and Goldman RD: Roles of vimentin in health and disease. Gene Dev 36: 391-407, 2022.
50. Cui H, Huang J, Lei Y, Chen Q, Hu Z, Niu J, Wei R, Yang K, Li H, Lu T, *et al*: Design and synthesis of dual inhibitors targeting snail and histone deacetylase for the treatment of solid tumour cancer. Eur J Med Chem 229: 114082, 2022.
51. Huang Y, Hong W and Wei X: The molecular mechanisms and therapeutic strategies of EMT in tumor progression and metastasis. J Hematol Oncol 15: 129, 2022.
52. Hao Y, Baker D and Ten DP: TGF-β-Mediated Epithelial-mesenchymal transition and cancer metastasis. Int J Mol Sci 20: 2767, 2019.

53. Brackenbury WJ and Isom LL: Na Channel β Subunits: Overachievers of the ion channel family. Front Pharmacol 2: 53, 2011.
54. Peng L, Gao R, Han L, Fu T and Bian C: Roles of β-catenin protein in non-small cell lung cancer (Review). Oncol Lett 30: 565, 2025.
55. Yu F, Yu C, Li F, Zuo Y, Wang Y, Yao L, Wu C, Wang C and Ye L: Wnt/β-catenin signaling in cancers and targeted therapies. Signal Transduct Tar 6: 307, 2021.
56. Fontana R, Mestre-Farrera A and Yang J: Update on Epithelial-mesenchymal plasticity in cancer progression. Annu Rev Pathol 19: 133-156, 2024.
57. Haddadin L and Sun X: Stem cells in cancer: From mechanisms to therapeutic strategies. Cells 14: 538, 2025.
58. Hu Q, Saleem K, Pandey J, Charania AN, Zhou Y and He C: Cell adhesion molecules in fibrotic diseases. Biomedicines 11: 1995, 2023.
59. Lin W, Fang J, Wei S, He G, Liu J, Li X, Peng X, Li D, Yang S, Li X, *et al*: Extracellular vesicle-cell adhesion molecules in tumours: Biofunctions and clinical applications. Cell Commun Signal 21: 246, 2023.
60. Morla S: Glycosaminoglycans and glycosaminoglycan mimetics in cancer and inflammation. Int J Mol Sci 20: 1936, 2019.
61. Xiao Y and Yu D: Tumor microenvironment as a therapeutic target in cancer. Pharmacol Ther 221: 107753, 2021.
62. Du T, Gao J, Li P, Wang Y, Qi Q, Liu X, Li J, Wang C and Du L: Pyroptosis, metabolism, and tumor immune microenvironment. Clin Transl Med 11: e492, 2021.
63. Elhanani O, Ben-Uri R and Keren L: Spatial profiling technologies illuminate the tumor microenvironment. Cancer Cell 41: 404-420, 2023.